

Microassembly of semiconductor three-dimensional photonic crystals

KANNA AOKI^{*†1}, HIDEKI T. MIYAZAKI², HIDEKI HIRAYAMA¹, KYOJI INOSHITA³, TOSHIHIKO BABA³, KAZUAKI SAKODA⁴, NORIO SHINYA² AND YOSHINOBU AOYAGI¹

¹Semiconductors Laboratory, RIKEN, 2-1 Hirosawa, Wako, Saitama 351-0198, Japan

²Materials Engineering Laboratory, National Institute for Materials Science, 1-2-1 Sengen, Tsukuba, Ibaraki 305-0047, Japan

³Department of Electrical and Computer Engineering, Yokohama National University, 79-5 Tokiwadai, Hodogaya, Yokohama 240-8501, Japan

⁴Nanomaterials Laboratory, National Institute for Materials Science, 3-13 Sakura, Ibaraki 304-0003, Japan

^{*}Present address: Research Center for Advanced Science Technology, University of Tokyo, 4-6 Komaba, Meguro, Tokyo 153-8505, Japan

[†]e-mail: kanna@iis.u-tokyo.ac.jp

Published online: 12 January 2003; corrected 14th January 2003 (details online); doi:10.1038/nmat802

Electronic devices and their highly integrated components formed from semiconductor crystals contain complex three-dimensional (3D) arrangements of elements and wiring. Photonic crystals, being analogous to semiconductor crystals, are expected to require a 3D structure to form successful optoelectronic devices. Here, we report a novel fabrication technology for a semiconductor 3D photonic crystal by uniting integrated circuit processing technology with micromanipulation. Four- to twenty-layered (five periods) crystals, including one with a controlled defect, for infrared wavelengths of 3–4.5 μm , were integrated at predetermined positions on a chip (structural error <50 nm). Numerical calculations revealed that a transmission peak observed at the upper frequency edge of the bandgap originated from the excitation of a resonant guided mode in the defective layers. Despite their importance, detailed discussions on the defective modes of 3D photonic crystals for such short wavelengths have not been reported before. This technology offers great potential for the production of optical wavelength photonic crystal devices.

Since the concept of the photonic bandgap (PBG) was introduced in 1987^{1,2}, the dream has been the creation of optical integrated circuits, in which zero-threshold lasers, sharp-bend waveguides or multiplexers are accumulated on one chip^{3,4}. Although 3D crystals are ideal to manipulate the flow of light at will, most of the efforts have been aimed at two-dimensional (2D) crystals, because they can be easily obtained using conventional semiconductor processing. Even with the weakness of imperfect PBG, 2D photonic crystals have surprisingly revealed their usefulness in the form of, for example, fibres⁵, waveguides^{6–11}, lasers^{12,13} and resonators^{14,15}. However, we still feel that 3D structures are essential for the realization of photonic crystal devices. A 3D arrangement of elements and wiring has been adopted in electronic devices to formulate highly integrated components. Thus, it is expected that future photonic devices will also need to adopt a 3D structure. For this to be possible, the use of 3D photonic crystals is fundamental.

Various trials^{16–30} have been conducted, and fabrication technologies for 3D crystals have come in many forms such as angle etching^{16–18}, colloidal precipitation^{19,20}, photopolymerization^{21–23}, and layer-by-layer methods^{24–30}. These structures show that perfect PBGs do exist in the real world, and greatly contributed to the increasing study of this field. The first successful 3D full-bandgap structure (Yablonovite) was realized by angle etching^{16–18}, which requires an incredibly high level of accuracy. The severe etching conditions tend to weaken the high symmetry of the structure, thus the optical properties of the crystals obtained tend to deteriorate. Colloidal precipitation methods^{19,20} are considered to be cheap for large-scale production of 3D photonic crystals. The artificial face-centred cubic crystal, which is formed by natural sedimentation of monodispersed spheres, is usually used as a mould for the semiconductor inversed structure to obtain full PBG. However, difficulties are encountered in the fabrication of large-scale ordered structures or with the introduction of arbitrary defects in the structure, because the formation of a periodical structure depends on natural precipitation of the microspheres. A defect that requires a combination of different materials, for example, a laser or a light-emitting diode, cannot be introduced. The inversed materials are

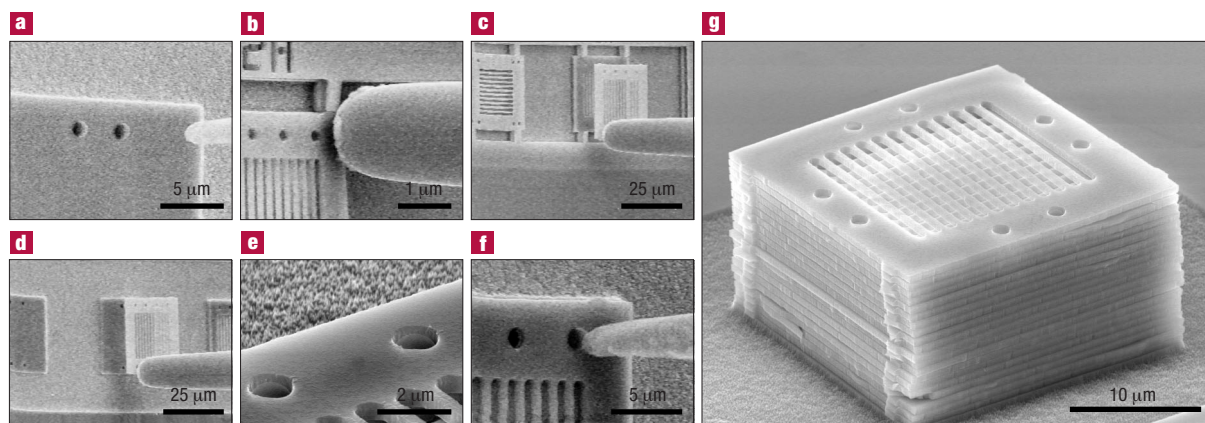


Figure 1 SEM images of micromanipulation. **a**, Two microspheres are inserted into pore openings of a substructure. **b**, A bridge of a plate is broken by pushing it with a probe tip. **c**, A photonic plate separated from a substrate is picked up with a probe. **d**, The separated plate is transferred to the substructure in **a**. **e**, The tops of microspheres inserted into the substructure guide the photonic plate into alignment by catching the holes of the plate. **f**, The 2D photonic plate is fixed on the substructure by inserting a microsphere into residual pore opening and two more microspheres are inserted into holes of the plate for stacking of the next layer. Pressure was adapted on the plate with the probe to promote self-bonding of plates. **g**, Side view of a 20-layer woodpile structure. The periods of rods, rod width and layer thickness are 1.4 μm , 0.37 μm and 0.5 μm , respectively. The size of the structure is 25 x 25 x 10 μm^3 and that of patterned region is 15 x 15 x 10 μm^3 .

limited to silicon and germanium, which are not suitable for light emission. The photopolymerization methods^{21–23} can construct a larger domain of ordered structures than the colloidal precipitation methods. Moreover, unlike the colloidal method, a predesignated defect could also be introduced. However, the approach of making a mould and replacing it with another material will encounter the same difficulty as the colloidal precipitation method. The most promising methods to date are thought to be layer-by-layer techniques^{24–30} that cleverly incorporate well-established integrated circuit processing techniques. Nevertheless, the complicated procedure, in addition to damage inflicted on the fine structure by frequent dry etching, polishing, and heating, made it difficult for further multilayering and the introduction of various materials and defects.

In short, existing technologies seem to share a common problem in the lack of flexibility in both design and materials, and have other concerns particular to each method. All of these technologies have concentrated on fabricating defectless large-scale crystals for the purpose of measuring the optical characteristics. Hence there is now the problem of proposing how the integration of multiple components can be achieved using these techniques.

In our approach, the desired 3D structures were initially sliced into several planar components. Each unit plate was prepared using a conventional integrated circuit processing procedure with subsequent assembly into 3D structures by micromanipulation. To achieve the correct lamination of components, fiducial points and fixtures were used (that is, precise ‘fixing’ positions were used in each plane such that the layering of the planes was exact). We report here the incorporation into the plate of circular holes with diameters twice the thickness of the plate, together with polystyrene microspheres whose diameters are similar to the fiducial holes. Because neighbouring plates have holes in identical positions, the layers are automatically aligned into the correct position by inserting microspheres into the holes. Adaptation of these procedures has resulted in several advantages over existing fabrication techniques. First, all unit plates can be prepared using a single sequence of an integrated circuit process without critical depth control in etching or polishing. Consequently, the procedure is simpler, with a lower risk of damage to the fine photonic patterns compared with existing techniques^{27–30}. Second, accurate alignment of lattices is

achieved irrespective of photonic patterns or materials. Therefore, any photonic structure can be assembled regardless of the materials or complexity of the photonic pattern. Third, because micromanipulation can handle objects of dimensions of the order of tens of nanometres, it is capable of introducing small items, such as emitters, into arbitrary positions in the structure.

For convenience in assembly, unit plates were sustained in air with narrow bridges. Indium phosphide (InP) was chosen as the material for the photonic crystal because InP group lasers have already won a reputation as a stable and high-power light source for 1.5 μm wavelength. Further, semiconductor materials can directly merge into existing semiconductor devices. Manufacturing details of the air-bridge unit plates used here—formed by a series of metalorganic chemical vapour deposition, electron-beam lithography, dry etching and wet etching—are given elsewhere³¹.

The unit plates were assembled using a micromanipulation system^{32,33} installed in the specimen chamber of a scanning electron microscope (SEM) with a field-emission gun. The plates were stacked on an InP wafer polished on both sides and patterned with fiducial holes whose diameter and positions were compatible with those of the first layer. SEM images of the assembly procedure are shown in Fig. 1. One sequence, as illustrated in Fig. 1a–f, was completed in a relatively short timescale of less than one hour. In the future, all the assembly processes could be automated by adapting a high-speed visual feedback system^{34,35} to bring the assembly speed to an industrial level. The key technique in this sequence is self-bonding of plates promoted by the pressure applied by the probe. In our previous report³¹, the 3D structure was maintained solely by the friction between a fiducial microsphere and the plates. Although aligned, stacked plates often peeled off by the adhesive force to a probe or an upper plate, therefore multilayering was quite difficult. In this work, we found that the plates never peeled off if they were pressed down for 30 minutes with a probe after the arrangement in the final position. It is known that adhesion force at a contact interface increases with the progress of time under SEM observation^{36,37}. The same mechanism seems to be working in our case. By introducing this self-bonding mechanism, multilayering over four layers became possible. In the previously reported methods^{27–30}, a high-temperature process was indispensable for each layering, but then deterioration of

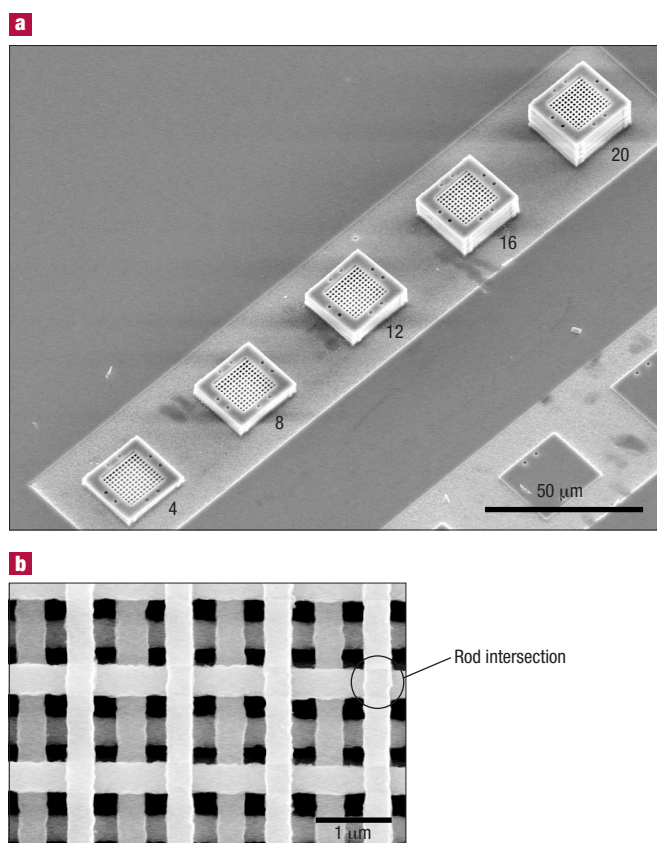


Figure 2 SEM images of 3D photonic crystals. **a**, Top view of 3D photonic crystals made of 4, 8, 12, 16, and 20 layers (corresponding to one to five periods). **b**, Surface view of the 20-layer woodpile structure shown in Fig. 1g.

fine structure and difficulty in the combination of materials of various melting points were inescapable problems. Such difficulties are completely avoidable by our technique. If more rigid bonding is required, high-temperature bonding should be applied only once after the structure is completed. Figure 2a shows the top view of arrayed 3D photonic crystals with 4, 8, 12, 16 and 20 layers. Figure 2b shows the top view of a 20-layered crystal; a side view of the crystal is presented in Fig. 1g. The periodical accuracy was in agreement with the four-layered crystal³¹, with a structural error of within 50 nm, as observed from Fig. 2b. Portions where the lattice intersects appear darker than that sustained in air, indicate that the layers are in intimate contact with each other. This demonstrates, to our knowledge, the first example of an arrangement of a predetermined number of 3D photonic crystals for use in optical wavelengths, with a fixed number of periods at pre-designated locations on a chip. Furthermore, this is also, to our knowledge, the first achievement in the production of crystals for optical wavelength of many periods whilst maintaining accuracy and yield. These features are essential for mass production and integration of photonic crystal-based devices. Additionally, it is desirable to achieve a stable supply of crystals of many periods for highly efficient devices, such as a resonator with a Q-factor as high as 10^3 – 10^4 (indicating long-lasting resonance)³⁸.

Reflection and transmission properties of the crystals were evaluated using a microscopic Fourier-transform infrared measurement system³³ at room temperature. The sample was characterized using an unpolarized beam that was collimated within a 20-degree divergent

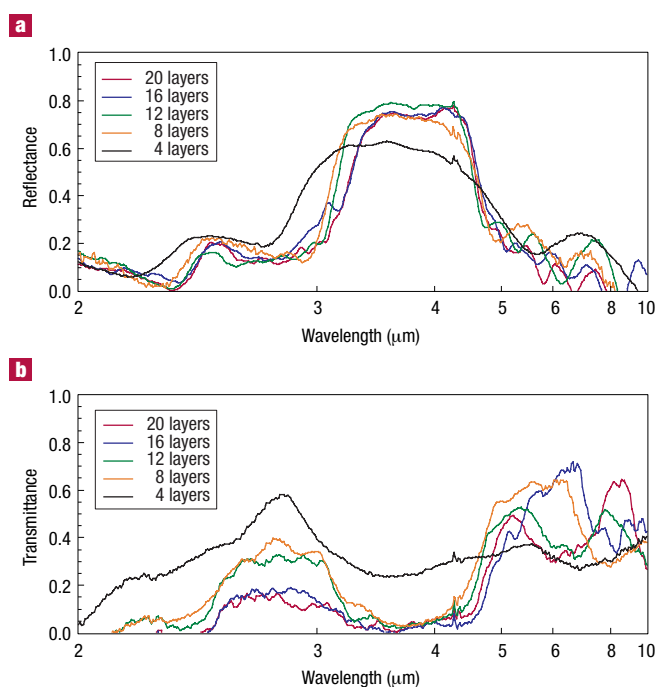


Figure 3 Optical properties of the fabricated 3D photonic crystals. **a**, Reflection spectra. **b**, Transmission spectra. The peaks appearing at 4.2 μm in all spectra are derived from absorption of carbon dioxide in air.

angle. The incident angles of the light were normal to and 20 degrees from the vertical direction of the (100) surface of the crystals, for the measurements of transmittance and reflectance, respectively. The area exposed to light was limited to the size of the photonic pattern using a rectangular slit. To determine absolute transmittance and reflectance, reference spectra were taken from an InP wafer polished on both sides, and a gold film that was deposited on the same InP wafer by sputter coating. The results are shown in Fig. 3. The fabricated crystals are estimated to have a stopband centring at around 4 μm by the plane-wave expansion method; the spectra of the crystals revealed such a stopband in the expected wavelength region. As the number of crystal periods was increased, the reflection peak became stronger and clearer. The intensities reached 75% with the eight-layer crystal and remained at similar values with thicker crystals. In the transmittance spectra, a gap appeared in the same wavelength region where the reflectance peaks were observed. The gap became deeper as the number of layers was increased, and the attenuation reached above 25 dB with the 20-layer crystal. This value is small compared with previously reported values^{27,28}. This was attributed to the small pattern size of the crystal and spread angle of incident light³¹. Preparation of larger crystals would be expected to deliver results equivalent to reported values. We can surely prepare large crystals with shorter periods, but would reach the size limitation of a relatively soft material such as InP. With other materials such as silicon (Si) and gallium arsenide (GaAs), or by hardening InP by adding GaAs, further enlargement and scaling down of the lattice constant would be possible. A gallium indium arsenide (GaInAs)/GaAs laser is also suitable for light-emitting devices for optical communication wavelengths. Silicon is useful for passive devices and excellent with electric devices. It is also possible to insert active components in Si-based devices.

Characteristic features were observed in the transmission regions in both the reflection and transmission spectra. Undulating structures appeared in the regions below 3.2 μm and above 4.5 μm , and their

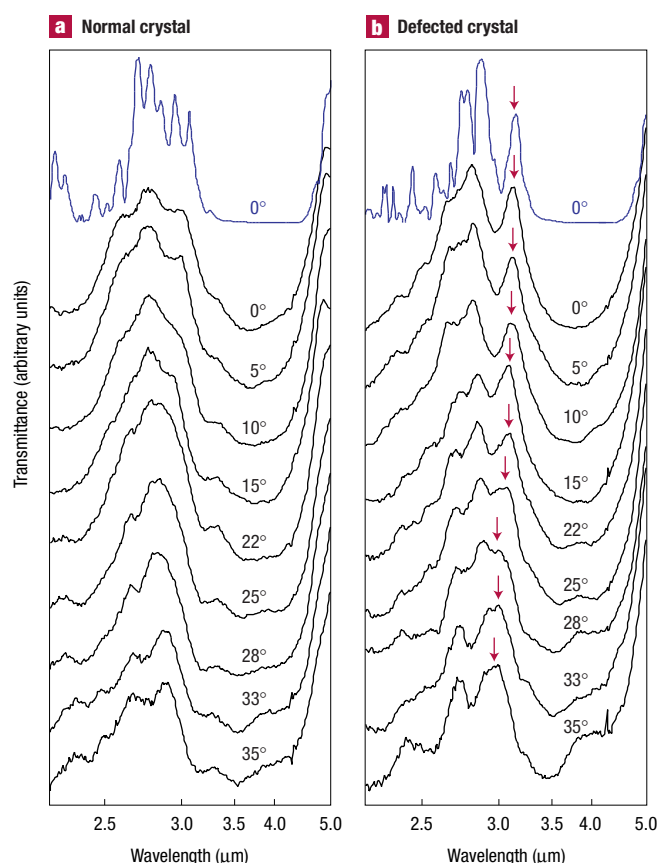


Figure 4 Transmission spectra of the normal and defective eight-layer photonic crystals. The incidence angle is systematically shifted from the (001) to (110) axes of the crystal orientation. Blue spectra are calculated transmittance by finite-difference time-domain calculation for normal incidence. **a**, Normal eight-layer crystal. **b**, Defective eight-layer crystal. The peak appearing at $3.2\ \mu\text{m}$ is derived from the resonance in the defect layers with incident light. The peaks at $4.2\ \mu\text{m}$ in all spectra are derived from absorption of carbon dioxide in air.

periods became shorter as the number of crystal layers increased. In particular, this feature is remarkable in the wavelength region longer than $4.5\ \mu\text{m}$ of reflection and at $2.5\text{--}3.2\ \mu\text{m}$ of transmission. Further, transmittance tends to diminish as the wavelength becomes shorter. Because there are no examples of an optical wavelength crystal of such a thickness, there are no reports describing the transmission regions of the spectrum. However, similar spectra have been reported for millimetre-wave scale multilayer crystals^{39,40}—the undulating structure and fall off in transmission in the high-frequency region in our results is in good agreement with these. The vibration is based on Fabry–Perot interference of reflections of both the front and back surfaces of a crystal⁴¹.

To demonstrate the flexibility in design of our technique, an eight-layer photonic crystal incorporating a defect was assembled on the same chip on which the crystals shown in Fig. 2a were integrated. Two layers with a rod width $d=0.47\ \mu\text{m}$ were sandwiched between two sets of three layers with $d=0.37\ \mu\text{m}$. Figure 4a,b shows the transmission spectra of the normal and defective eight-layer photonic crystals, respectively. The PBG shifted from $3\text{--}4.5\ \mu\text{m}$ to $3.2\text{--}5\ \mu\text{m}$ through incorporation of defect layers. A shift of the gap to a lower frequency as the dielectric filling ratio becomes larger is as expected⁴². One remarkable difference between the normal and defective crystal transmission spectra was a

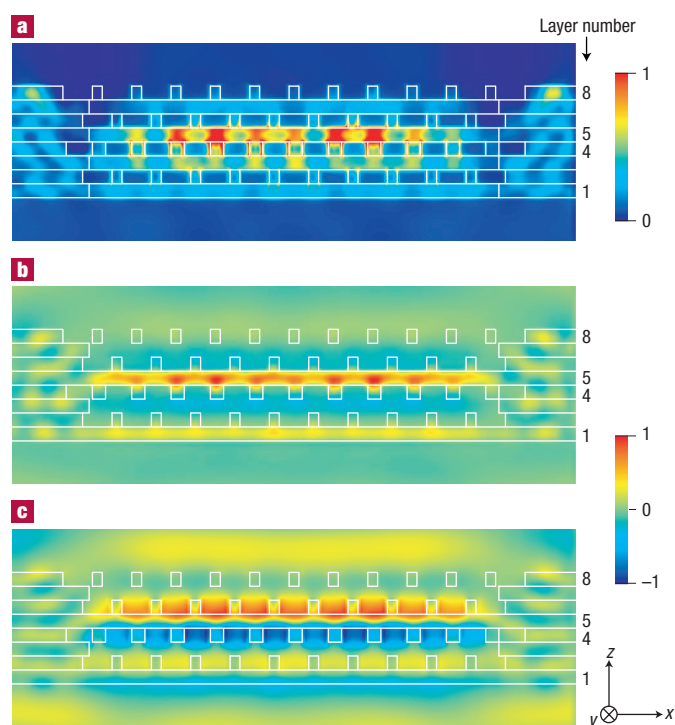


Figure 5 Electromagnetic fields in the $x\text{--}z$ plane of the defective eight-layer photonic crystal at the peak transmission frequency calculated by the finite difference time domain method. The x , y and z axes are indicated in the figure. The x -polarized plane wave is incident on the crystal from the bottom along the z axis. **a**, Energy distribution, which was obtained by integrating electric and magnetic energies to the direction of y axis and time. The colour scale represent the strongest (red) to weakest (blue) intensity. Perspective outlines of the crystal structure are superimposed on the diagram (white lines). **b**, The y component of the magnetic field is plotted in the $x\text{--}z$ plane on the linear scale. The $x\text{--}z$ plane passes along the centre of the rod of the fifth layer. **c**, The x -component of the electric field in the same plane as in **b**. The colour scale for **b** and **c** represents positive (red) to negative (blue).

sharp peak that appeared at the high-frequency edge of the PBG (bottom of the conduction band) in the spectra of the defective crystal. This peak gradually shifted to a higher frequency and merged with other peaks as the incidence angle was increased, as highlighted by the arrows in Fig. 4b. A systematic 3D finite-difference time-domain calculation was performed to investigate the origin of this peak. Theoretical spectra calculated for normal incidence are also illustrated as blue plots in Fig. 4a,b. The positions of the PBG for both crystals and the transmission peak at $3.2\ \mu\text{m}$ of the defective crystal were reproduced well in the calculated spectra. Major changes in spectral features corresponding to an increase in the incidence angle were also reproduced in the theoretical plots (data not shown). Sharp fringes appearing in the range of $2.5\text{--}3.0\ \mu\text{m}$ in the calculated spectra appear to be smoothed out in the observed spectra due to divergence of the incident light. By calculation of the electromagnetic fields, it was found that energy concentrated in the rods parallel to the polarization of the incident light in the modified layers, that is, the fourth or the fifth layer, at the transmission peak at $3.2\ \mu\text{m}$. The energy distribution in the $x\text{--}z$ plane for x -polarized incident wave at the peak frequency is shown in Fig. 5a. Because the rods of the fifth layer are parallel to the x axis, energy is localized into the rods of the fifth layer. The magnetic and electric fields at the maximum moment at the same frequency are shown in Fig. 5b and c, respectively. The y

component of the magnetic field is localized in the centre of the rod in the fifth layer. In contrast, the x component of the electric field is anti-symmetrically distributed at the upper and lower surfaces of the rod. Moreover, there was a 90° phase difference between them. These are typical characteristics of the zeroth transverse magnetic mode for slab waveguides. To conclude, a resonant guided mode is excited in the rods of the defect layers by the external fields polarized in parallel with the rod. The light is subsequently coupled out to the opposite side by this defect mode and is observed as a transmission peak.

In the past, models magnified to millimetre-wave scale³⁸ have been used to investigate detailed defect modes of photonic crystals. Verification of these defects by a real-size model is indispensable for the realization of photonic crystals, because the introduction of such defects is limited using conventional fabrication technologies. The establishment of our technology has enabled a detailed relationship to be explored between the structure and photonic characteristics using real-scale crystals. Also a technology that can perform stable assembly in the order of a micrometre or submicrometre scale is indispensable, not only to the field of photonic crystal devices, but to the field of micro electromechanical systems (MEMS; the expression 'micro system technologies' (MST) is more popular in Europe)⁴³, which is a key-technology in miniaturizing and upgrading electronic devices. Furthermore, other photonic crystal fabrication techniques can explore new possibilities by incorporating our technology⁴⁴.

In this article, we have fabricated prototype crystals for wavelengths longer than optical communications to confirm the essential soundness of our idea. In the next stage, we will go on to the production of larger crystals for optical communication wavelengths, introduction of more complicated defects such as lasing elements, multilevel crossing and branched waveguides, and integration of various elements on one chip.

Received 3 October 2002; accepted 25 November 2002; published 12 January 2003; corrected 14th January 2003 (details online).

References

- Yablonovitch, E. Inhibited spontaneous emission in solid-state physics and electronics. *Phys. Rev. Lett.* **58**, 2059–2062 (1987).
- John, S. Strong localization of photons in certain disordered dielectric superlattices. *Phys. Rev. Lett.* **58**, 2486–2489 (1987).
- Hirayama, H., Hamano, T., & Aoyagi, Y. Novel surface emitting laser diode using photonic band-gap crystal cavity. *Appl. Phys. Lett.* **69**, 791–793 (1996).
- Joannopoulos, J. D., Villeneuve, P. R. & Fan, S. Photonic crystals: Putting a new twist on light. *Nature* **386**, 143–149 (1997).
- Knight, J. C., Birks, T. A., Russell, P. St. J. & Atkin, D. M. All-silica single-mode optical fiber with photonic crystal cladding. *Opt. Lett.* **21**, 1547–1549 (1996).
- Krauss, T. F., De La Rue, R. M. & Brand, S. Two-dimensional photonic-bandgap structures operating at near-infrared wavelengths. *Nature* **383**, 699–702 (1996).
- Labilloy, D. *et al.* Quantitative measurement of transmission, reflection, and diffraction of two-dimensional photonic band gap structures at near-infrared wavelengths. *Phys. Rev. Lett.* **79**, 4147–4150 (1997).
- Lin, S. Y., Chow, E., Hietala, V., Villeneuve, P. R. & Joannopoulos, J. D. Experimental demonstration of guiding and bending of electromagnetic waves in a photonic crystal. *Science* **282**, 274–276 (1998).
- Baba, T., Fukaya, N. & Yonekura, J. Observation of light propagation in photonic crystal optical waveguides with bends. *Electron. Lett.* **35**, 654–655 (1999).
- Notomi, M. *et al.* Extremely large group-velocity dispersion of line-defect waveguides in photonic crystal slabs. *Phys. Rev. Lett.* **87**, 253902 (2001).
- Sugimoto, Y. *et al.* Fabrication and characterization of different types of two-dimensional AlGaAs photonic crystal slabs. *J. Appl. Phys.* **91**, 922–929 (2002).
- Painter, O. *et al.* Two-dimensional photonic band-gap defect mode laser. *Science* **284**, 1819–1821 (1999).
- Noda, S., Yokoyama, M., Imada, M., Chutinan, A. & Mochizuki, M. Polarization mode control of two-dimensional photonic crystal laser by unit cell structure design. *Science* **293**, 1123–1125 (2001).
- Labilloy, D. *et al.* Demonstration of cavity mode between two-dimensional photonic-crystal mirrors. *Electron. Lett.* **33**, 1978–1980 (1997).
- Noda, S., Chutinan, A. & Imada, M. Trapping and emission of photons by a single defect in a photonic bandgap structure. *Nature* **407**, 608–610 (2000).
- Yablonovitch, E. *et al.* Donor and acceptor modes in photonic band structure. *Phys. Rev. Lett.* **67**, 3380–3383 (1991).
- Cheng, C. C. & Scherer, A. Fabrication of photonic band-gap crystals. *J. Vac. Sci. Technol. B* **13**, 2696–2700 (1995).
- Chelnokov, A., Wang, K., Rowson, S., Garoche, P. & Lourtioz, J. M. Near-infrared Yablonovitch-like photonic crystals by focused-ion-beam etching of macroporous silicon. *Appl. Phys. Lett.* **77**, 2943–2945 (2000).
- Blanco, A. *et al.* Large-scale synthesis of a silicon photonic crystal with a complete three-dimensional bandgap near 1.5 micrometres. *Nature* **405**, 437–440 (2000).
- Vlasov, Y. A., Bo, X. Z., Sturm, J. C. & Norris, D. J. On-chip natural assembly of silicon photonic bandgap crystals. *Nature* **414**, 289–293 (2001).
- Sun, H. B., Matsuo, S. & Misawa, H. Three-dimensional photonic crystal structures achieved with two-photon-absorption photopolymerization of resin. *Appl. Phys. Lett.* **74**, 786–788 (1999).
- Campbell, M., Sharp, D. N., Harrison, M. T., Denning, R. G. & Turberfield, A. J. Fabrication of photonic crystals for the visible spectrum by holographic lithography. *Nature* **404**, 53–56 (2000).
- Shoji, S. & Kawata, S. Photofabrication of three-dimensional photonic crystals by multibeam laser interference into a photopolymerization resin. *Appl. Phys. Lett.* **76**, 2668–2670 (2000).
- Ho, K. M., Chan, C. T., Soukoulis, C. M., Biswas, R. & Sigalas, M. Photonic band gaps in three dimensions: New layer-by-layer periodic structures. *Solid State Commun.* **89**, 413–416 (1994).
- Özbay, E. *et al.* Measurement of a three-dimensional photonic band gap in a crystal structure made of dielectric rods. *Phys. Rev. B* **50**, 1945–1948 (1994).
- Chelnokov, A., Rowson, S., Lourtioz, J. M., Duvillaret, L. & Coutaz, J. L. Terahertz characterisation of mechanically machined 3D photonic crystal. *Electron. Lett.* **33**, 1981–1982 (1997).
- Lin, S. Y. *et al.* A three-dimensional photonic crystal operating at infrared wavelengths. *Nature* **394**, 251–253 (1998).
- Noda, S., Tomoda, K., Yamamoto, N. & Chutinan, A. Full three-dimensional photonic bandgap crystals at near-infrared wavelengths. *Science* **289**, 604–606 (2000).
- Feigel, A. *et al.* Chalcogenide glass-based three-dimensional photonic crystals. *Appl. Phys. Lett.* **77**, 3221–3223 (2000).
- Fleming, J. G., Lin, S. Y., El-Kady, I., Biswas, R. & Ho, K. M. All-metallic three-dimensional photonic crystals with a large infrared bandgap. *Nature* **417**, 52–55 (2002).
- Aoki, K. *et al.* Three-dimensional photonic crystals for optical wavelengths assembled by micromanipulation. *Appl. Phys. Lett.* **81**, 3122–3124 (2002).
- Morishita, H. & Hatamura, Y. Development of ultra micro manipulator system under stereo SEM observation. *Proc. 1993 IEEE/RSJ Int. Conf. Intelligent Robots and Systems* **3**, 1717–1721 (1993).
- Miyazaki, H. T., Miyazaki, H., Ohtaka, K., & Sato, T. Photonic band in two-dimensional lattices of micrometer-sized spheres mechanically arranged under a scanning electron microscope. *J. Appl. Phys.* **87**, 7152–7158 (2000).
- Kasaya, T., Miyazaki, H., Saito, S. & Sato, T. Micro object handling under SEM by vision-based automatic control. *Proc. 1999 IEEE Int. Conf. Robotics and Automation* **2**, 2189–2196 (1999).
- Namiki, A., Nakabo, Y., Ishii, I. & Ishikawa, M., 1-ms sensory-motor fusion system. *IEEE/ASME Trans. Mechatron.* **5**, 244–252 (2000).
- Miyazaki, H. T., Tomizawa, Y., Saito, S., Sato, T., & Shinya, N. Adhesion of micrometer-sized polymer particles under a scanning electron microscope. *J. Appl. Phys.* **88**, 3330–3340 (2000).
- Saito, S., Miyazaki, H. T., Sato, T. & Takahashi, K. Kinematics of mechanical and adhesive micro-manipulation under a scanning electron microscope. *J. Appl. Phys.* **92**, 5140–5149 (2002).
- Özbay, E., Tuttle, G., Sigalas, M., Soukoulis, C. M. & Ho, K. M. Defect structures in a layer-by-layer photonic band-gap crystal. *Phys. Rev. B* **51**, 13961–13965 (1995).
- Wada, M., Doi, Y., Inoue, K., Haus, J. W. & Yuan, Z. A simple-cubic photonic lattice in silicon. *Appl. Phys. Lett.* **70**, 2966–2968 (1997).
- Aoki, T. *et al.* Terahertz time-domain study of a pseudo-simple-cubic photonic lattice. *Phys. Rev. B* **64**, 45106 (2001).
- Sakoda, K. Transmittance and Bragg reflectivity of two-dimensional photonic lattices. *Phys. Rev. B* **52**, 8992–9002 (1995).
- Joannopoulos, J. D., Meade, R. D. & Winn, J. N. *Photonic Crystals* (Princeton Univ. Press, New Jersey, 1995).
- Bishop, D., Gammel, P. & Giles, C. R. The little machines that are making it big. *Phys. Today* **54**, 38–44 (2001).
- García-Santamaría, F. *et al.* Nanorobotic manipulation of microspheres for on-chip diamond architectures. *Adv. Mater.* **14**, 1144–1147 (2002).

Acknowledgements

We thank T.Sato, H. Morishita and Y. Hatamura for their support. This work has been supported by a Grant-in-Aid for Scientific Research from the Ministry of Education, Culture, Sports, Science, and Technology of Japan. K.A. gratefully acknowledges a fellowship 'President's Special Research Grant' provided by RIKEN.

Correspondence and requests for materials should be addressed to K.A.

Competing interests statement

The authors declare that they have no competing financial interests.